Electronic Supplementary Material (ESI) for Journal of Materials Chemistry C.

Supplementary Information

Use of the time constant related parameter f_{max} to calculate the activation energy of bulk conduction in ferroelectrics.

F. Yang,* L. Li, P. Wu, E. Pradal-Velázquez, H. K. Pearce and D. C. Sinclair*

Department of Materials Science & Engineering, University of Sheffield, S1 3JD, UK.

* Corresponding authors: fan.yang@sheffield.ac.uk; d.c.sinclair@sheffield.ac.uk

1. XRD patterns and lattice parameters

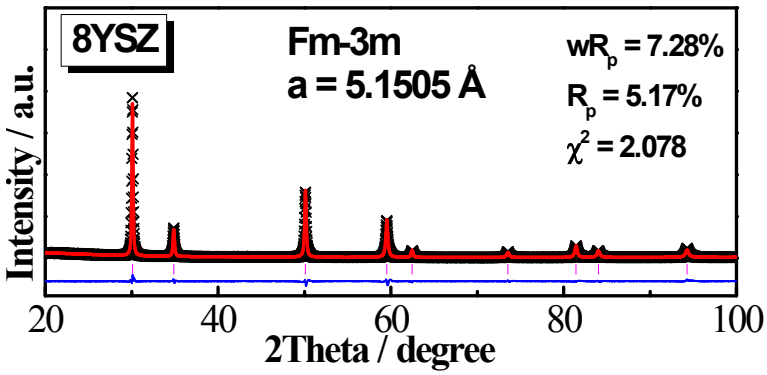

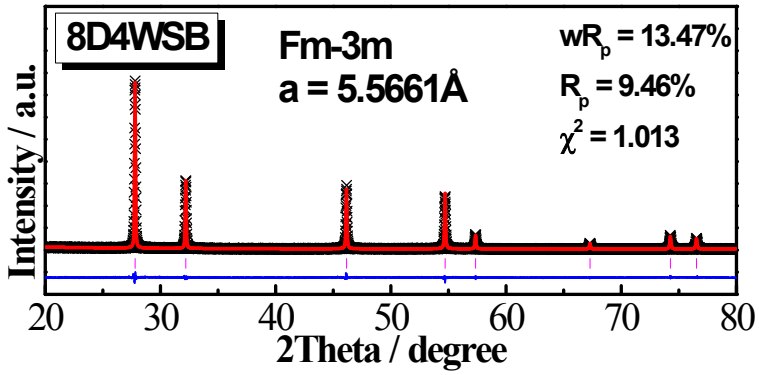

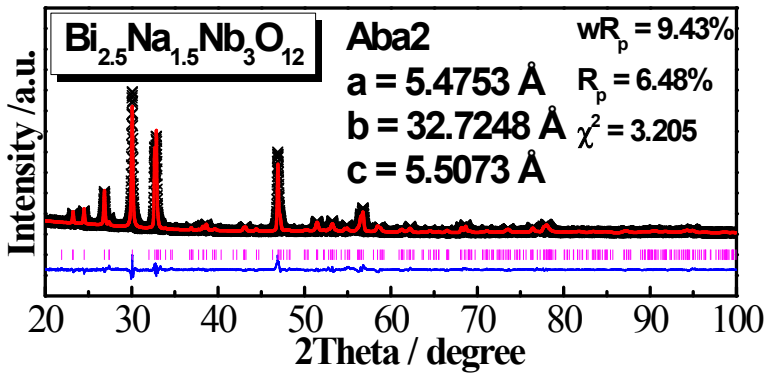

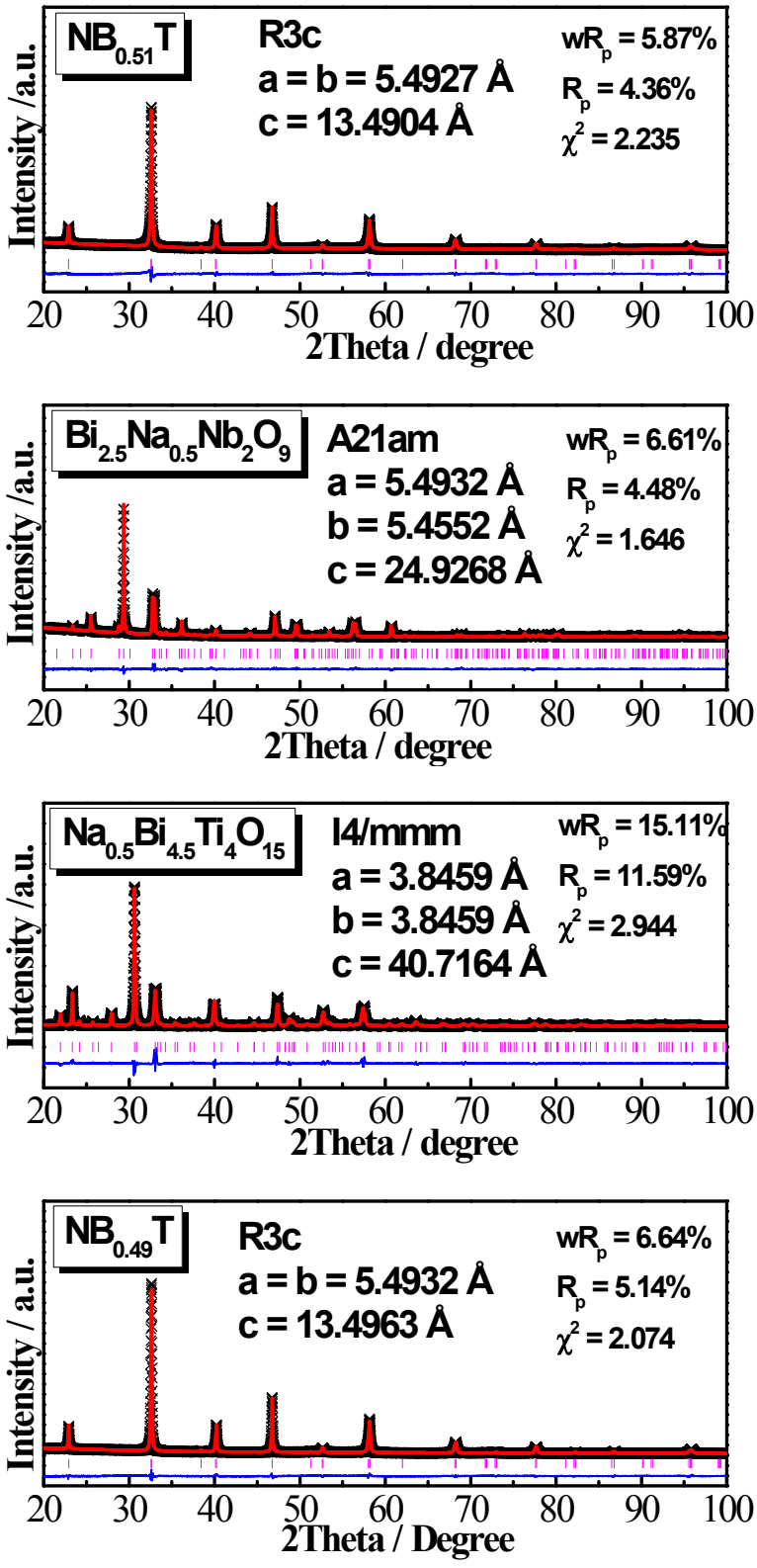

Fig.S1 XRD patterns and Rietveld refinements of the materials investigated in this study. The cross symbols in each figure represent the observed pattern and the solid line shows the calculated fit. The reflection marker for each structure is shown as vertical lines with the

difference pattern below the diffraction pattern. Space group, lattice parameters and quality of fit are indicated in each figure.

2. Permittivity-temperature and tanδ-temperature profiles

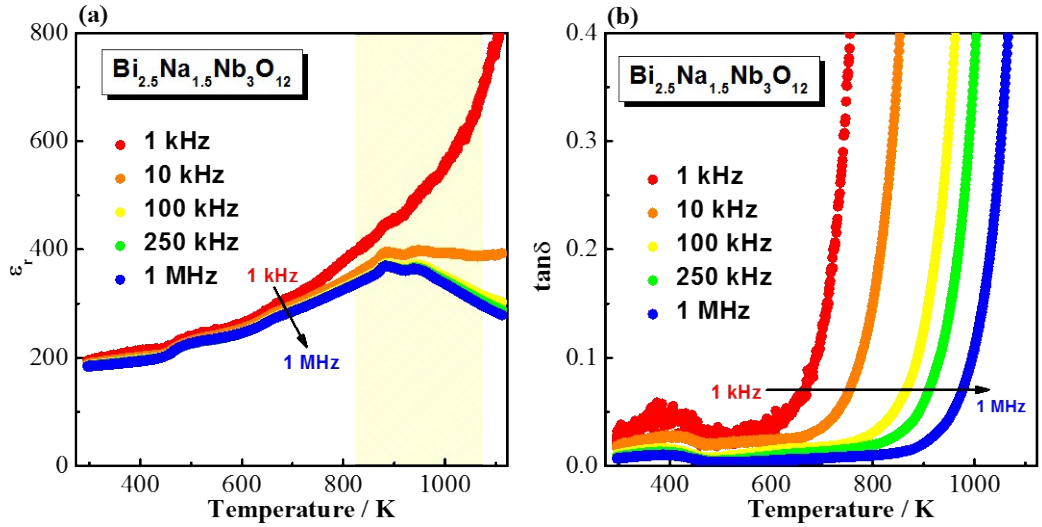

Fig.S2 (a) Permittivity-temperature and (b) dielectric loss-temperature profiles of $Bi_{2.5}Na_{1.5}Nb_3O_{12}$ at various frequencies. The shaded region in (a) indicates the temperature range where impedance data were collected.

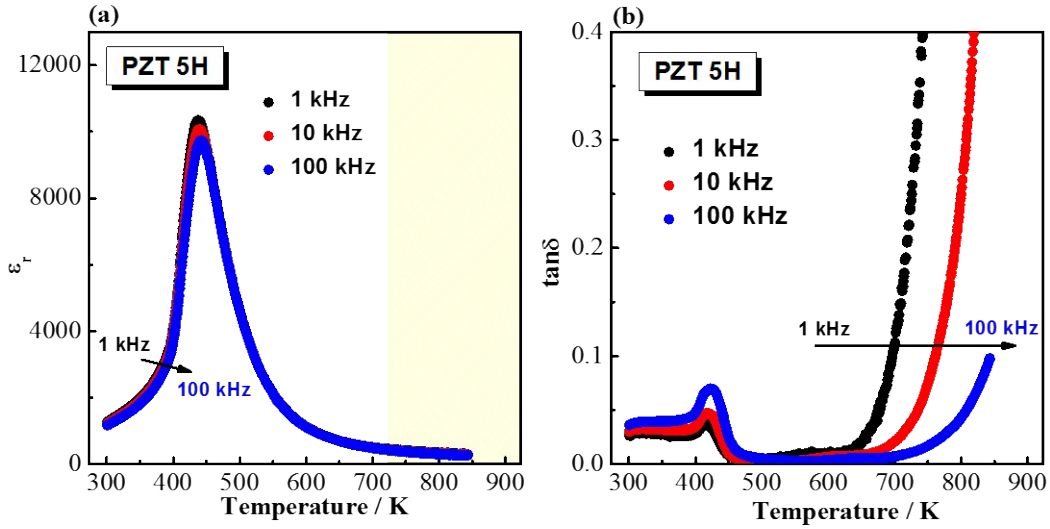

Fig.S3 (a) Permittivity-temperature and (b) dielectric loss-temperature profiles of "soft" PZT 5H at various frequencies. The shaded region in (a) indicates the temperature range where impedance data were collected.

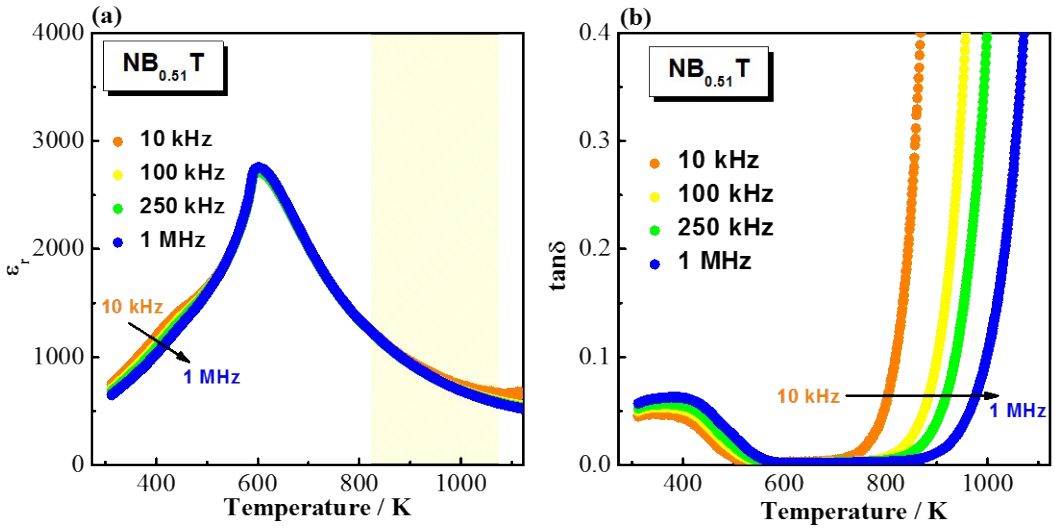

Fig.S4 (a) Permittivity-temperature and (b) dielectric loss-temperature profiles of $Na_{0.5}Bi_{0.51}TiO_{3.015}$ ($NB_{0.51}T$) at various frequencies. The shaded region in (a) indicates the temperature range where impedance data were collected.

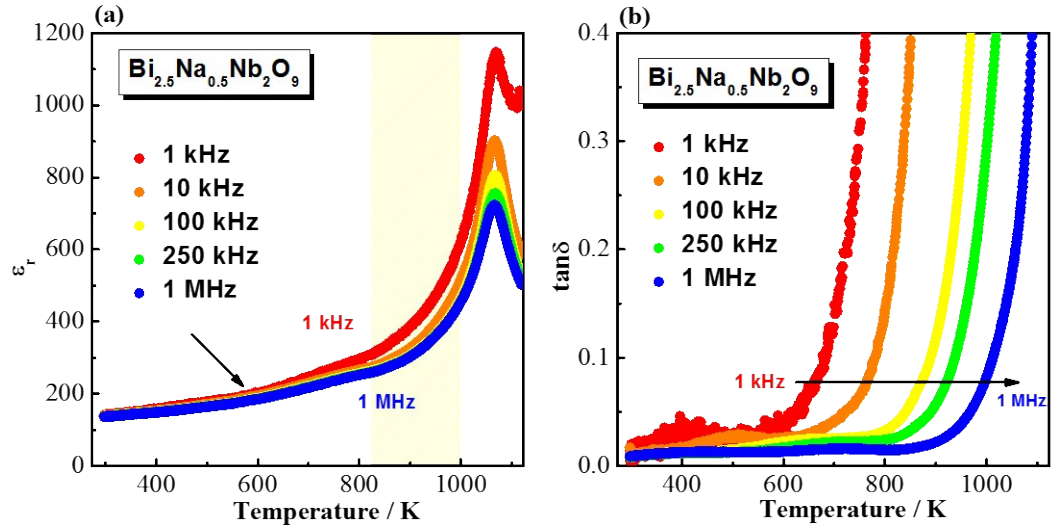

Fig.S5 (a) Permittivity-temperature and (b) dielectric loss-temperature profiles of $Bi_{2.5}Na_{0.5}Nb_2O_9$ at various frequencies. The shaded region in (a) indicates the temperature range where impedance data were collected.

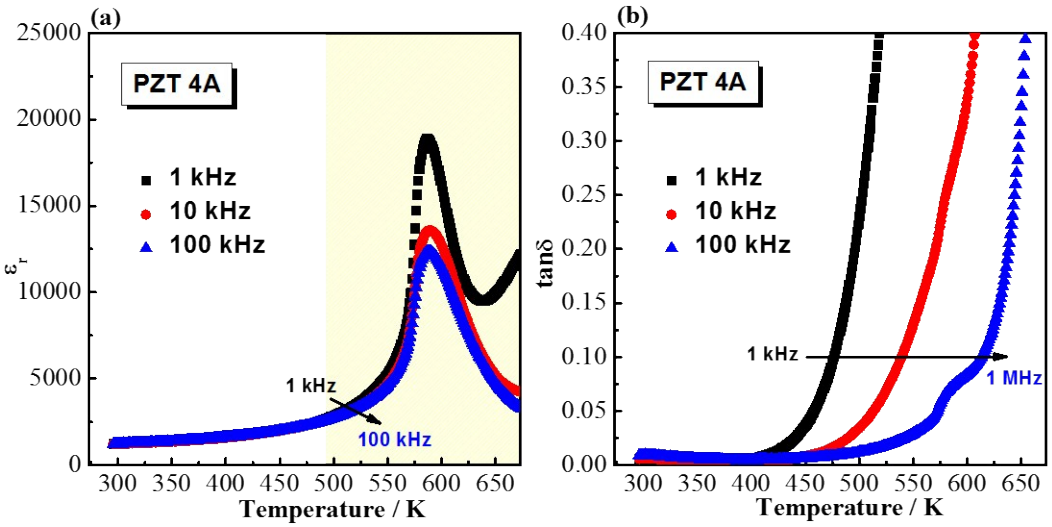

Fig.S6 (a) Permittivity-temperature and (b) dielectric loss-temperature profiles of "hard" PZT 4A at various frequencies. The shaded region in (a) indicates the temperature range where impedance data were collected.

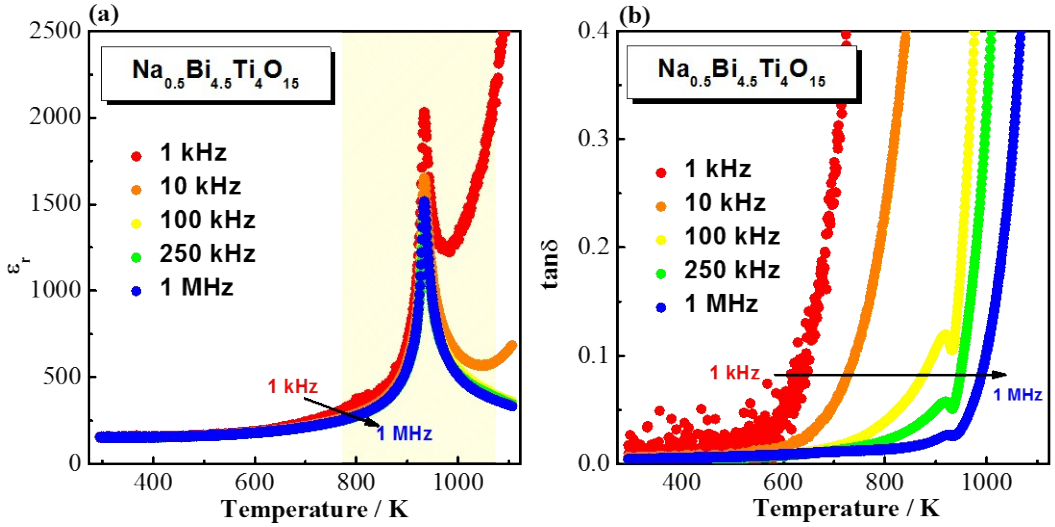

Fig.S7 (a) Permittivity-temperature and (b) dielectric loss-temperature profile of $Na_{0.5}Bi_{4.5}Ti_4O_{15}$ at various frequencies. The shaded region in (a) indicates the temperature range where impedance data were collected.

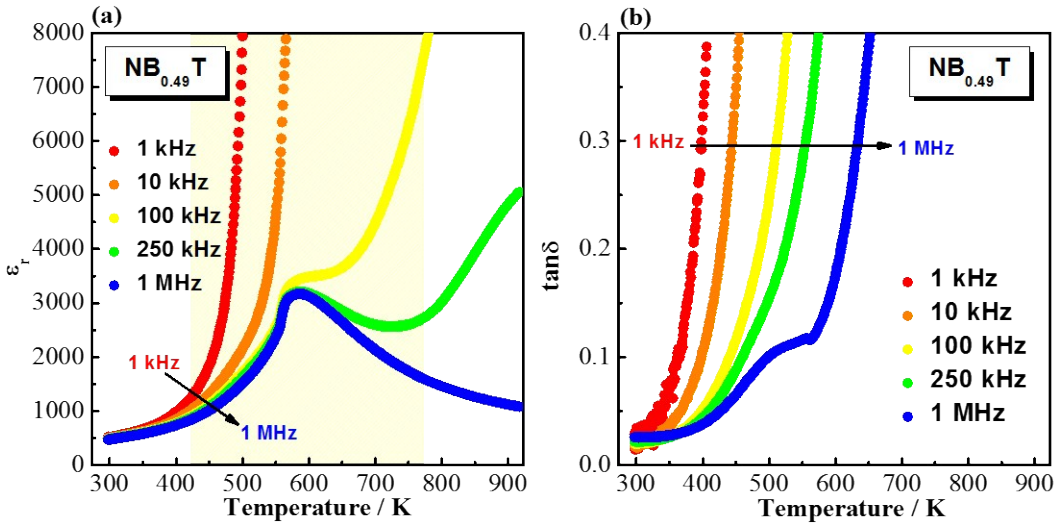

Fig.S8 (a) Permittivity-temperature and (b) dielectric loss-temperature profile of $Na_{0.5}Bi_{0.49}TiO_{2.985}$ ($NB_{0.49}T$) at various frequencies. The shaded region in (a) indicates the temperature range where impedance data were collected.

3. Other examples

1) 8D4WSB (δ_0)

The Z* plot for 8W4DSB in Fig.S9a shows an arc corresponding to the bulk response and a spike at low frequency corresponding to the electrode effect which is a signature of ionic conduction. The lack of a grain boundary response in 8D4WSB can be related to the purity of the raw materials and/or a microstructural feature but it is out of the scope of this paper. The M''-log*f* spectroscopic plots show a single Debye peak, corresponding to the bulk response. The M'' peak shifts to higher frequency with increasing temperature with a very small decrease in the peak height, Fig.S9b. The permittivity shows weak temperature dependence, increasing from 65 to 67 over a range of ~100 K, Fig.S9c. Arrhenius plots for the bulk conductivity, σ_b, and the time constant related parameter f_{max}, both show a linear relationship with T^{-1}, with the same activation energy of 0.93 eV, Fig.S9d.

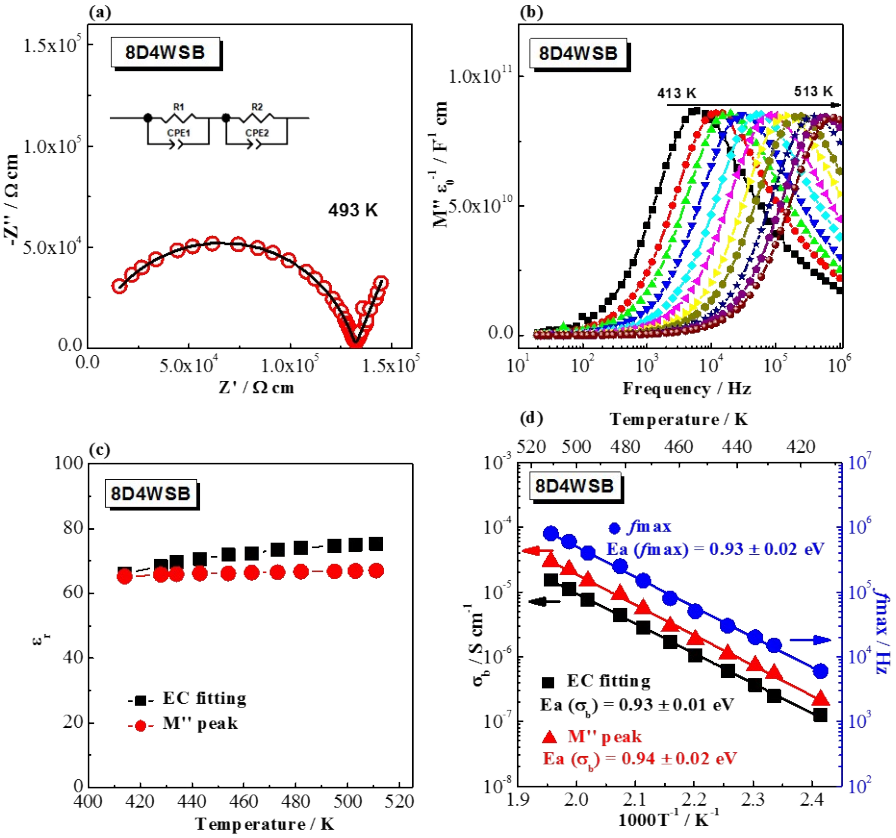

Fig.S9. (a) Z* plot for 8D4WSB measured at 493 K. Red open circles are the experimental data and the black line is the fitting curve using the equivalent circuit (EC) shown in the inset figure; (b) M''-log$f$ plots from 413 to 513 K at intervals of 10 K; (c) relative permittivity as a function of temperature; and (d) Arrhenius plots for the bulk conductivity, σ_b, and the time constant related parameter f_{max} and their associated activation energies $E_a(\sigma_b)$ and $E_a(f_{max})$, respectively.

2) $NB_{0.51}T$ (large δ, i.e., $\delta_5 - \delta_7$, $T_2 > T_1 >> T_m$)

Z* plots for electronically insulating $NB_{0.51}T$ show a single arc, which can be fitted by one R-CPE element, Fig.S10a and its inset. The capacitance value associated with this arc is consistent with a bulk response [1]. The single Debye peak in the M''-log$f$ spectroscopic plots shifts to higher frequency with increasing temperature with a continuous increase in peak height, Fig.S10b, and consequently a continuous decrease in permittivity from 823 to 1073 K, Fig.S10c. Arrhenius plots for σ_b and f_{max} both show a linear relationship with T^{-1} but with different activation energies, i.e., $E_a(\sigma_b) \sim 1.7$ eV and $E_a(f_{max}) \sim 1.95$ eV, Fig.S10d.

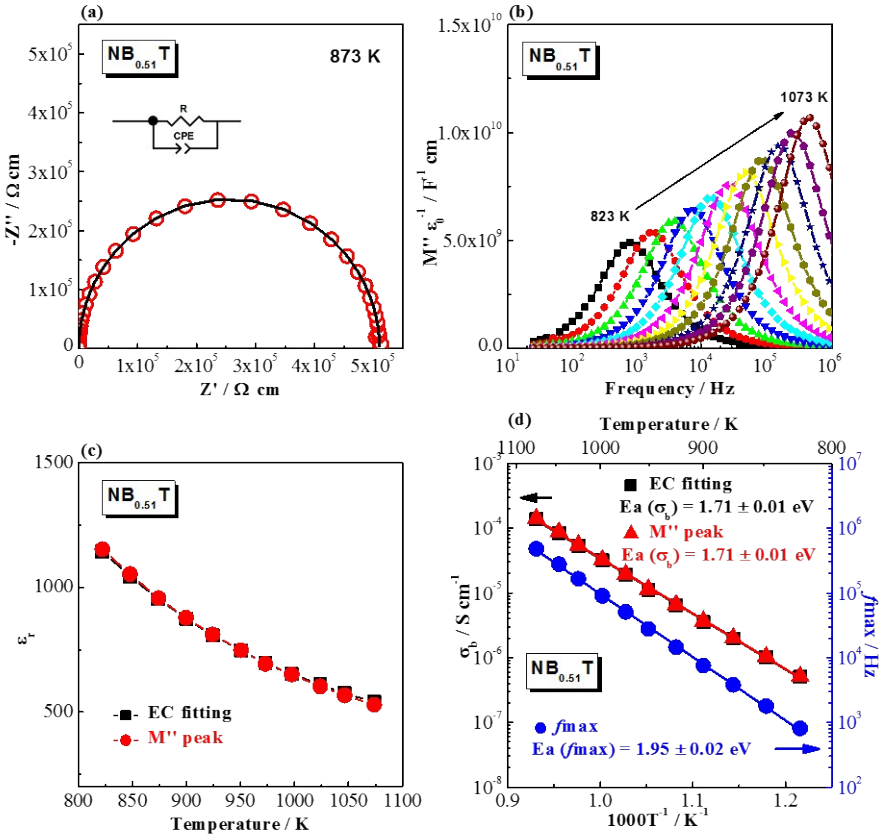

Fig.S10. (a) Z* plot for $NB_{0.51}T$ measured at 873 K. Red open circles are the experimental data and the black line is the fitting curve using the equivalent circuit (EC) shown in the inset figure; (b) M''-log*f* plots from 823 to 1073 K at intervals of 25 K; (c) relative permittivity as a function of temperature; and (d) Arrhenius plots for the bulk conductivity, σ_b, and the time constant related parameter f_{max} and their associated activation energies $E_a(\sigma_b)$ and $E_a(f_{max})$, respectively.

3) **$Na_{0.5}Bi_{4.5}Ti_4O_{15}$** (large δ, i.e., $\delta_5 - \delta_7$, $T_1 < T_m < T_2$)

The Z* plot for $Na_{0.5}Bi_{4.5}Ti_4O_{15}$ shows two arcs, Fig.S11a. The larger arc in the higher frequency range corresponds to the bulk response and the smaller arc in the lower frequency range corresponds to either a grain boundary or an electrode effect according to the associated capacitance value (~ 1.7×10^{-7} F). The impedance data can be fitted by two R-CPE elements connected in series, inset in Fig.11a. The M''-log*f* spectroscopic plots show a single Debye peak, which shifts to higher frequency with increasing temperature from 773 to 873 K, and then moves backward to lower frequency with increasing temperature in a narrow temperature range between 873 and 898 K before it starts to shift to higher frequency again from 898 to 1073 K, Fig.S11b. The M'' peak height shows a significant decrease with increasing temperature, reaching a minimum at 898 K before increasing rapidly at higher temperatures.

The permittivity-temperature profile shows a sharp peak at 898 K, Fig.S11c. The Arrhenius plot, $\log\sigma_b$ -T^{-1} shows a linear relationship with E_a of 1.54 eV; however, the $\log f_{max}$ -T^{-1} relationship presents multiple features: below 873 K and above 973 K, $\log f_{max}$ shows a linear relationship with T^{-1}, which gives E_a of 0.91 and 1.94 eV, respectively. Between 873 and 973 K, $\log f_{max}$ first decreases with increasing T^{-1} reaching its lowest value at ~ 948 K and then slightly increases with increasing T^{-1}, showing a sharp downward bend, Fig.S11d.

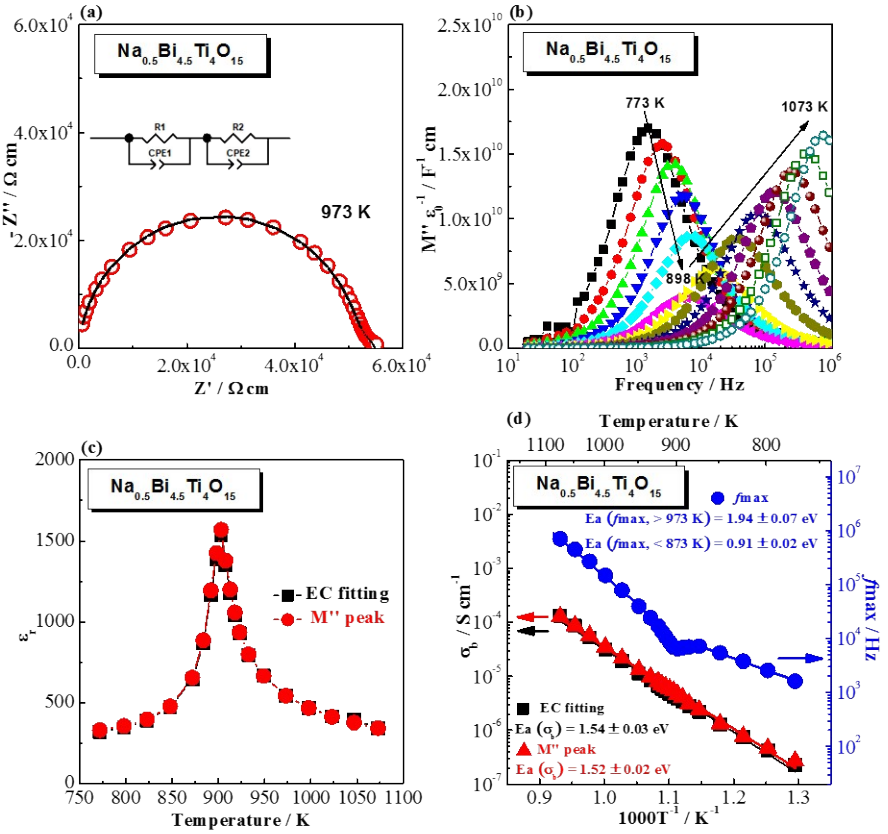

Fig.S11. (a) Z* plot for $Na_{0.5}Bi_{4.5}Ti_4O_{15}$ measured at 973 K. Red open circles are the experimental data and the black line is the fitting curve using the equivalent circuit (EC) shown in the inset figure; (b) M''-log*f* plots from 773 to 1073 K at intervals of 25 K; (c) relative permittivity as a function of temperature; and (d) Arrhenius plots for the bulk conductivity, σ_b, and the time constant related parameter f_{max} and their associated activation energies $E_a(\sigma_b)$ and $E_a(f_{max})$, respectively.

4. Conduction mechanisms

1) $Bi_{2.5}Na_{1.5}Nb_3O_{12}$

Fig.S12 shows a Z* plot for $Bi_{2.5}Na_{1.5}Nb_3O_{12}$ measured at 973 K in nitrogen, air and oxygen. It reveals the arc associated with the bulk response was smallest when measured in nitrogen (low pO_2) and largest when measured in oxygen (high pO_2). No obvious Warburg spike is observed in the low frequency region (< 0.1 Hz, inset figure). The pO_2 dependence and absence of an electrode spike suggest a predominately *n*-type electronic conduction mechanism in $Bi_{2.5}Na_{1.5}Nb_3O_{12}$ according to the equilibrium $O^{2-} \leftrightarrow \frac{1}{2}O_2 + 2e$. [2]

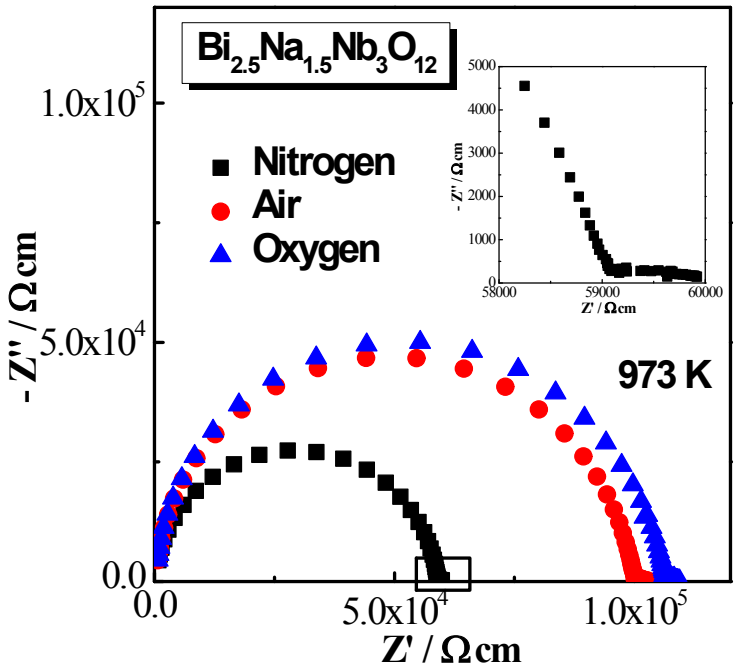

Fig. S12. Z* plot for $Bi_{2.5}Na_{1.5}Nb_3O_{12}$ measured at 973 K in nitrogen, air and oxygen. The inset figure is an expanded view of the low frequency region indicated by the rectangle.

2) PZT 5H

Fig.S13 shows a Z* plot for PZT 5H measured at 873 K in nitrogen, air and oxygen. It reveals the arc associated with the bulk response to be smallest when measured in oxygen (high pO_2) and largest when measured in nitrogen (low pO_2). An expanded view of the low frequency region (inset figure) shows the Warburg impedance from electrode effect. The pO_2 dependence and the electrode spike suggest a mixed conduction mechanism in PZT 5H. Charge carriers are oxygen ions and holes.

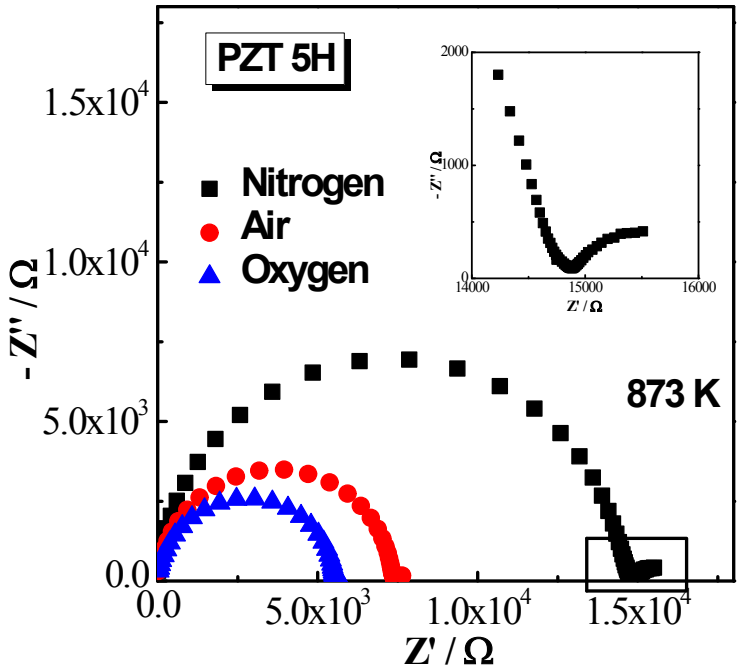

Fig. S13. Z* plot for PZT 5H measured at 873 K in nitrogen, air and oxygen. The inset figure is an expanded view of the low frequency region indicated by the rectangle.

3) $Bi_{2.5}Na_{0.5}Nb_2O_9$

Fig.S14 shows a Z* plot for $Bi_{2.5}Na_{0.5}Nb_2O_9$ measured at 973 K in nitrogen, air and oxygen. It reveals the bulk arc to be smallest when measured in nitrogen (low pO_2) and largest when measured in oxygen (high pO_2). There is no obvious Warburg spike observed in the low frequency region (< 0.1 Hz, inset figure). This suggests a predominately *n*-type electronic conduction mechanism in $Bi_{2.5}Na_{0.5}Nb_2O_9$.

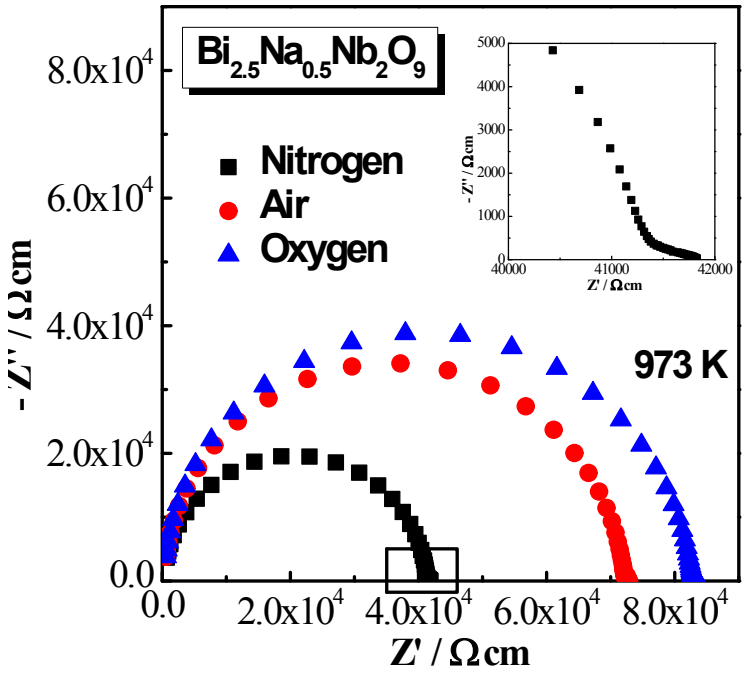

Fig. S14. Z* plot for $Bi_{2.5}Na_{0.5}Nb_2O_9$ measured at 973 K in nitrogen, air and oxygen. The inset figure is an expanded view of the low frequency region indicated by the rectangle.

4) PZT 4A

Fig.S15 shows a Z* plot for PZT 4A measured at 523 K in nitrogen, air and oxygen. It reveals the bulk arc to be smallest when measured in oxygen (high pO_2) and largest when measured in nitrogen (low pO_2). There is no obvious Warburg impedance in the low frequency region, as shown by the expanded view (inset figure). The pO_2 dependence and the electrode spike suggest a predominant electronic conduction mechanism in PZT 4A with holes as the charge carriers.

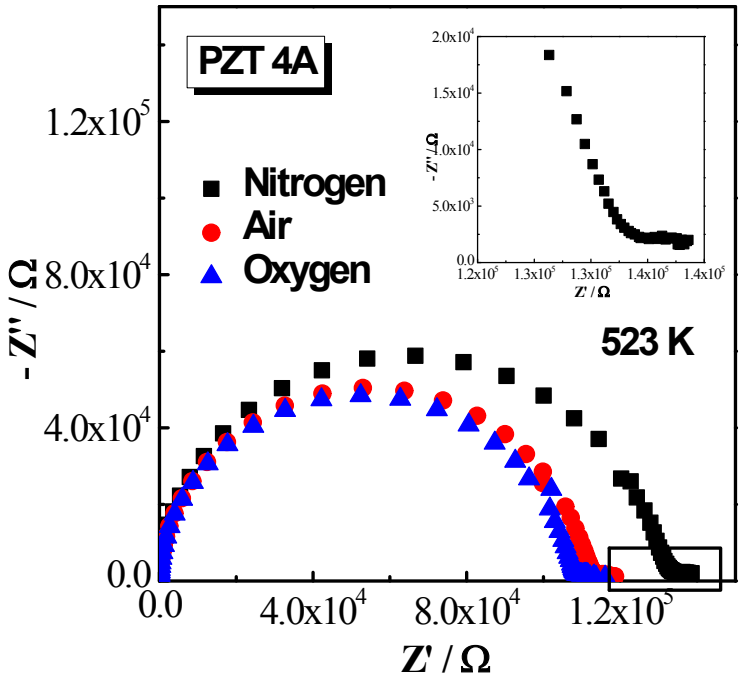

Fig. S15. Z* plot for PZT 4A measured at 523 K in nitrogen, air and oxygen. The inset figure is an expanded view of the low frequency region indicated by the rectangle.

5) $Na_{0.5}Bi_{4.5}Ti_4O_{15}$

Fig.S16 shows a Z* plot for $Na_{0.5}Bi_{4.5}Ti_4O_{15}$ measured at 973 K in nitrogen, air and oxygen. It reveals the bulk arc to be smallest when measured in nitrogen (low pO_2) and largest when measured in oxygen (high pO_2). An expanded view of the low frequency region (< 0.1 Hz, inset figure) shows a modest Warburg spike. The pO_2-dependence of the bulk response and the presence of a Warburg impedance from an electrode effect suggest a mixed ionic-electronic conduction mechanism in $Na_{0.5}Bi_{4.5}Ti_4O_{15}$. Charge carriers are electrons and oxygen ions. Transport number measurement by electromotive force (EMF) method shows an ionic transport number of 0.3[3], which supports the conclusion from impedance.

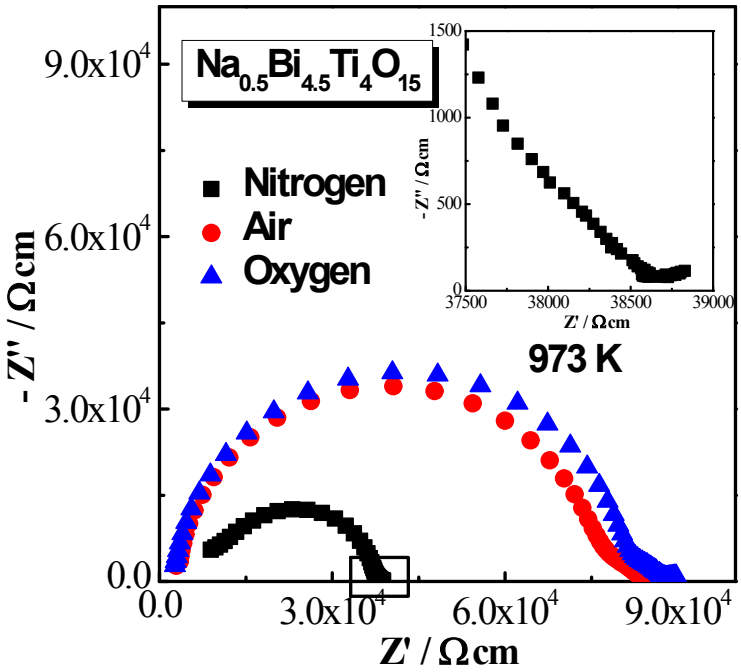

Fig. S16. Z* plot for $Na_{0.5}Bi_{4.5}Ti_4O_{15}$ measured at 973 K in nitrogen, air and oxygen. The inset figure is an expanded view of the low frequency region indicated by the rectangle.

References

[1] M. Li, M. J. Pietrowski, R. A. De Souza, H. Zhang, I. M. Reaney, S. N. Cook, J. A. Kilner and D. C. Sinclair, "A family of oxide ion conductors based on the ferroelectric perovskite $Na_{0.5}Bi_{0.5}TiO_3$", Nature Materials 13 (2014) 31-35.

[2] Y. Liu and A. R. West, "Voltage-dependent resistance of undoped rutile, TiO_2, ceramics", Applied Physics Letters 103 (2013) 263508.

[3] L. Li and D. C. Sinclair, unpublished results.